scientific reports

Check for updates

OPEN

Precision dosing of recombinant vaccinia vaccine via pillar-guided microneedle patch confers SARS-CoV-2 immunity

Kotaro Shobayashi[1], Jongho Park[2], Hoshimi Aoyagi[2], Fumihiko Yasui[3], Michinori Kohara[3] & Beomjoon Kim[2]✉

Recent advances in microneedle array patch (MAP) technology have highlighted its potential for efficient and accessible vaccine delivery. In this study, we developed a pillar-guided MAP (PG-MAP) loaded with a recombinant vaccinia virus (r-DIs-S) expressing the SARS-CoV-2 spike (S) gene. Our fabrication method enabled precise localization of a high viral titer (> 9.4 ± 1.8 × 10⁶ PFU per patch), as verified by plaque assay. In vivo immunization in mice demonstrated that the r-DIs-S-loaded PG-MAP elicited robust S-protein-specific IgG and neutralizing antibody responses. Upon SARS-CoV-2 challenge, all PG-MAP-immunized mice survived and maintained their body weight, whereas the control groups experienced severe results. These results demonstrated that the PG-MAP platform enables precise dosing, maintains viral stability, and induces potent protective immunity, offering a promising alternative for decentralized, minimally invasive vaccination strategies against emerging infectious diseases.

Keywords COVID-19 vaccination, Microneedle array patch, Vaccinia virus vector, R-DIs-S, Minimally invasive administration

Future pandemics are not a question of "*if*", but "*when*." The ongoing emergence of infectious diseases and viral variants that outpace current vaccine distribution infrastructure underscores the urgent need for efficient, durable, and widely accessible vaccination strategies. Although current platforms, such as mRNA vaccine[1], adenovirus vector vaccines[2], and inactivated whole-virus formulations[3], have significantly reduced COVID-19-related morbidity and mortality, challenges still persist. These include waning immunity, limited cross-protection against emerging variants, and logistical hurdles in the repeated administration.

To address these limitations, Kohara et al. previously developed a recombinant vaccinia virus strain (r-DIs-S) derived from the highly attenuated Dairen I minute-pock variant (DIs), engineered to express the SARS-CoV-2 spike (S) protein[4]. Attenuated vaccinia strains, such as DIs, are compelling vaccine vectors due to their safety, immunogenicity, and prior success in smallpox eradication[5]. The DIs strain, characterized by ~ 15.4 kb genomic deletion, exhibits a restricted host range and lacks the ability to replicate in most mammalian cells[6,7]. They demonstrated that r-DIs-S induces robust humoral and cellular immune responses in both mice and macaques, providing broad protection from early SARS-CoV-2 strains to Omicron BA.1 variants (TY38-873)[4]. Importantly, the immunity was durable, lasting at least six months post-vaccination in murine models. Furthermore, intradermal (ID) delivery of r-DIs-S has been shown to circumvents pre-existing immunity to vaccinia vectors, which can limit the efficacy of viral vector vaccines[8]. The recombinant vaccinia vaccine can be administered multiple times. Vaccinia virus vaccines are reportedly most effective when administered through epidermal or intradermal inoculation. However, conventional ID delivery methods, such as the Mantoux technique, require skilled medical personnel and are difficult to standardize in mass immunization settings[9,10]. Scarification using bifurcated needles, once used during smallpox campaigns, suffers from imprecise dosing, inefficient vaccine use, and risk of needlestick injuries[11].

Microneedle array patches (MAPs) have emerged as promising alternatives to address these limitations. MAPs offer painless application[12,13], improved thermostability[13,14], dose-sparing capabilities[15], and the potential

[1]Department of Precision Engineering, School of Engineering, The University of Tokyo, Tokyo 113-8656, Japan. [2]Institute of Industrial Science, The University of Tokyo, Tokyo 153-8505, Japan. [3]Tokyo Metropolitan Institute of Medical Science, Tokyo 156-0057, Japan. ✉email: bjoonkim@iis.u-tokyo.ac.jp

for self-administration[16,17]. Among microneedle designs, including hollow, coated, porous, hydrogel, and dissolvable types, dissolving microneedles (dMNs) have advanced furthest toward clinical adoption owing to their safety and usability profiles[18–23]. General advantages and disadvantages of hollow, coated and dissolving microneedles are described in Supplementary Information 1. However, integrating live viral vaccines into dMNs remains technically challenging owing to issues such as imprecise dosing, antigen instability, and viral loss during fabrication of the dMNs.

Various strategies have been proposed to localize payloads at microneedle tips and minimize their diffusion into the backing layer[24,25]. Alternatively, hydrophobic backing materials have been used to minimize drug solubility in the backing layer, effectively reducing drug diffusion and partitioning from dMNs to the backing layer[26]. Another approach involves the inclusion of tiny air bubbles or porous layers that can separate each microneedle tip from the patch backing after application[27]. Arrowhead-shaped dMNs represent another design, where drug-loaded arrowheads are fabricated separately and then attached to supportive shafts in the patch backing during a later stage of the fabrication process[28]. Yet these methods often result in inconsistent release profiles or require complex fabrication steps that hinder scalability. To overcome these challenges, we developed a novel pillar-guided MAP (PG-MAP) design using a stereolithographically printed backing layer with engineered pillars for precise dose delivery (Fig. 1). This approach enables the localization of vaccine payloads exclusively at the microneedle tips, improving both drying efficiency and viral titer stability.

In this study, we demonstrated that r-DIs-S-loaded PG-MAPs retain high viral titer stability during fabrication and induce SARS-CoV-2-specific immune responses *in vivo*. Furthermore, immunization induced by PG-MAP enabled complete protection against lethal SARS-CoV-2 challenge in a murine model. In murine immunization studies, MAP-based administration induced immunogenicity, characterized by an immune response similar to conventional skin scarification vaccination. Our findings establish PG-MAP as a promising platform for the thermostable, minimally invasive, and scalable delivery of recombinant virus vector vaccines, particularly under limited cold-chain resources.

Results & discussion

Optimization of vaccine formulation

Determination of virus titer for MN based delivery

Neutralizing antibody responses serve as key indicators of vaccine efficacy and are positively correlated with the administered dose. In murine models, intradermal administration of the vaccinia virus has been shown to induce dose-dependent increases in both virus-specific IgG and neutralizing antibodies across a range of 10^6 to 10^8 PFU[29]. The traditional replicative smallpox vaccine, delivered via a bifurcated needle, typically contains ~ 2×10^5 PFU[30]. Notably, clinical dilution studies have demonstrated that doses with 10-fold lower titers (~ 10^4 PFU per dose) can still induce seroconversion in over 97% of individuals[31]. The Modified Vaccinia Ankara (MVA-BN) vaccine (Jynneos, Imvamune, Imvanex) is a highly attenuated vaccinia virus similar to DIs. A comparison was made between the subcutaneous administration of the liquid formulation of the MVA-BN vaccine at the standard dose (1×10^8 $TCID_{50}$ [50% tissue culture infectious dose]) and the intradermal administration of the vaccine at one-fifth of the standard dose (2×10^7 $TCID_{50}$)[32,33]. Based on these findings, we selected a target dose of 1×10^7 PFU of r-DIs-S for murine immunization aiming to assess the immunogenicity of microneedle-based delivery.

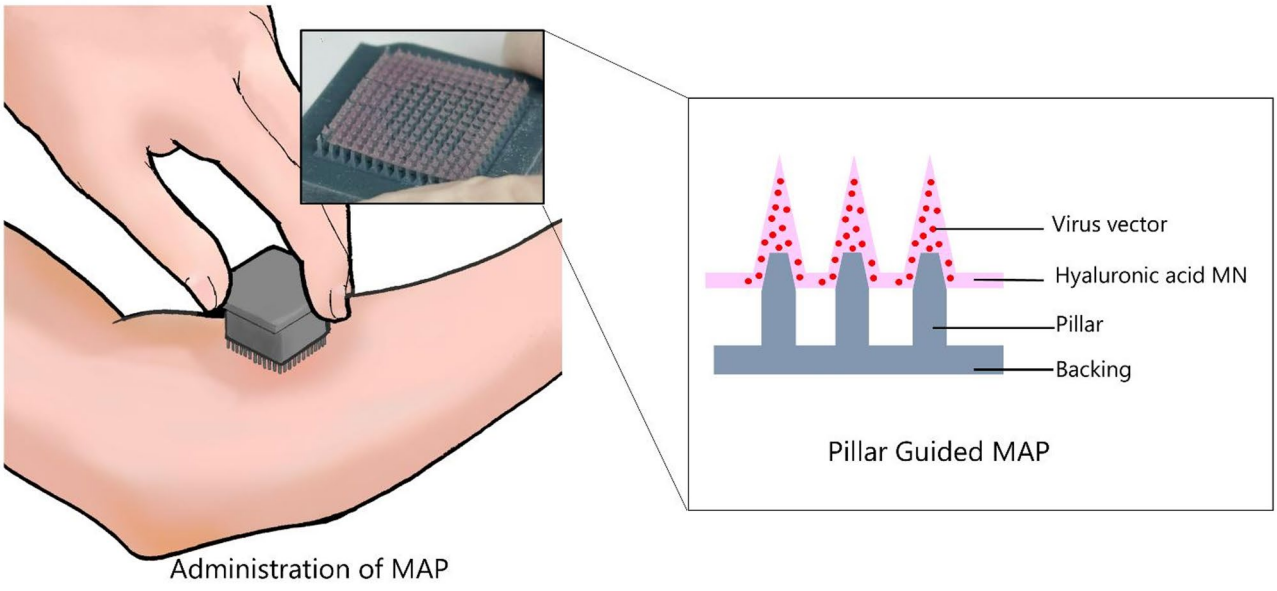

Fig. 1. Schematic illustration showing the administration of MAP for r-DIs-S vaccination.

Effect of HA concentration on viral stability

We selected hyaluronic acid (HA) due to its broad biomedical applications, FDA approval, and favorable properties as a biocompatible and biodegradable material[34]. We first investigated the effect of hyaluronic acid concentration on viral titer stability. Formulations containing 5%, 10%, 15% and 20% HA showed a dose-dependent improvement in viral stability, with the 20% HA formulation yielding the highest preservation of infectious titer (Fig. 2a). This result corresponds with previous reports indicating that HA forms a protective matrix around virions, mitigating titer loss under ambient conditions[35]. We selected the 15% HA formulation for subsequent experiments to balance viral preservation with handling advantages such as the precision dispensing of HA solution onto the PDMS mold and to minimize virus loss during solution.

Meanwhile, increasing solute concentration in the external liquid increases the osmotic pressure across the virus solvent interface, imposing stress such as surface tension effects[36]. Therefore, to preserve maximum viral activity in dried preparations for industrial applications, it is expected that rapid drying of the virus formulation might minimize the exposure time of viral particles to harmful osmotic fluctuations. Although the 20% HA formulation showed the highest stability within our tested range, further increasing the HA concentration may surpass the threshold. Future studies will evaluate this concentration and the dependence of osmotic stress to identify the balance between viral preservation and formulation handling properties.

To evaluate the influence of temperature during MAP fabrication, we measured viral titers following storage of HA–virus solutions at either 4–25 °C for 6 h, considering the preparation of MAPs including the dispensing and drying process. Viral titers by plaque assays demonstrated a pronounced effect of working temperature on viral stability. Samples stored at 4 °C retained approximately 71% of the initial titer, whereas those at 25 °C retained only 41% (Fig. 2b). These findings indicated that lower temperatures during the dispensing and drying steps during MAP fabrication can enhance the stability of the vaccinia virus. From these results, we confirmed that minimizing thermal exposure during fabrication is critical for maximizing vaccine potency.

(a) Effect of hyaluronic acid (HA) concentration on the viral viability of DIs after drying. Plaque assay analysis showing the impact of HA concentration on the stability of DIs in the formulation. Increasing the HA concentration from 5% to 20% progressively enhanced viral titer stability. Data represent mean ± SD ($n = 4$). P-values were calculated using one-way ANOVA (*$p < 0.05$; ns, not significant). (b) Viral titer changes at different storage temperatures (4 °C vs. 25 °C) over 6 h. Data represent mean SD ($n = 4$). P-values were calculated using one-way ANOVA (*$p < 0.05$; ns, not significant). Samples stored at 4 °C retained approximately 71% of the initial viral titer, whereas storage at 25 °C resulted in the reduction, with only 41% of the titer preserved.

Development and evaluation of the pillar guided MAP

Conventional dissolvable microneedle array patches (MAPs) often suffer from imprecise dose control, prolonged drying times, and inefficient payload localization issues. When water-soluble materials are used for the backing layer, they cause re-dissolution of the needle and unwanted spread of the vaccine material into the backing. These limitations lead to disadvantages, such as longer drying times, which reduce vaccine activity and cause vaccine loss. To address these limitations, we developed a pillar-guided MAP (PG-MAP) system featuring a 3D-printed backing layer with integrated pillar structures (Fig. 3a–b). These pillars enhance the loading of the vaccine to the tip and minimize the loss of the vaccine into the backing layer.

Design of PG-MAP

The backing layer, fabricated using a stereolithography (SLA) printer, incorporated a pillar insertion design. The backing layer was designed with pillars of 300 µm base diameter and 1,000 µm length, arranged in a 14 × 14 array. We designed the tip of the pillar to be 400 µm to maximize the surface contact with the HA solution when inserted into the microneedle cavities (Fig. 3a). Optical microscope analysis of five independent backings showed that the mean pillar tip height (P_{tip_height}) was 368 ± 16 µm, the pillar length (P_{length}) was 1003 ± 18 µm and the pillar base (P_{base}) was 312 ± 14 µm ($n = 5$) (Fig. 3b).

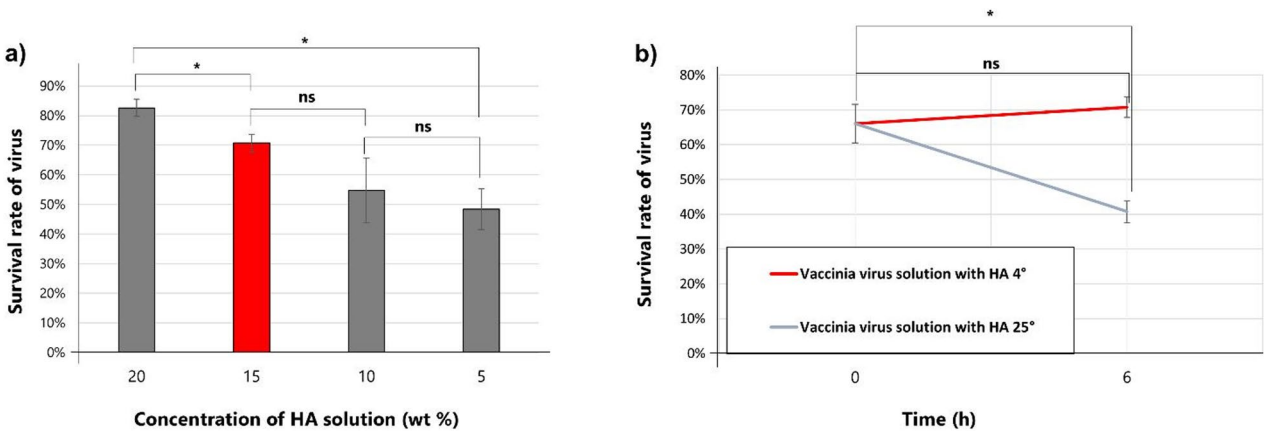

Fig. 2. Optimization of vaccine formulation conditions.

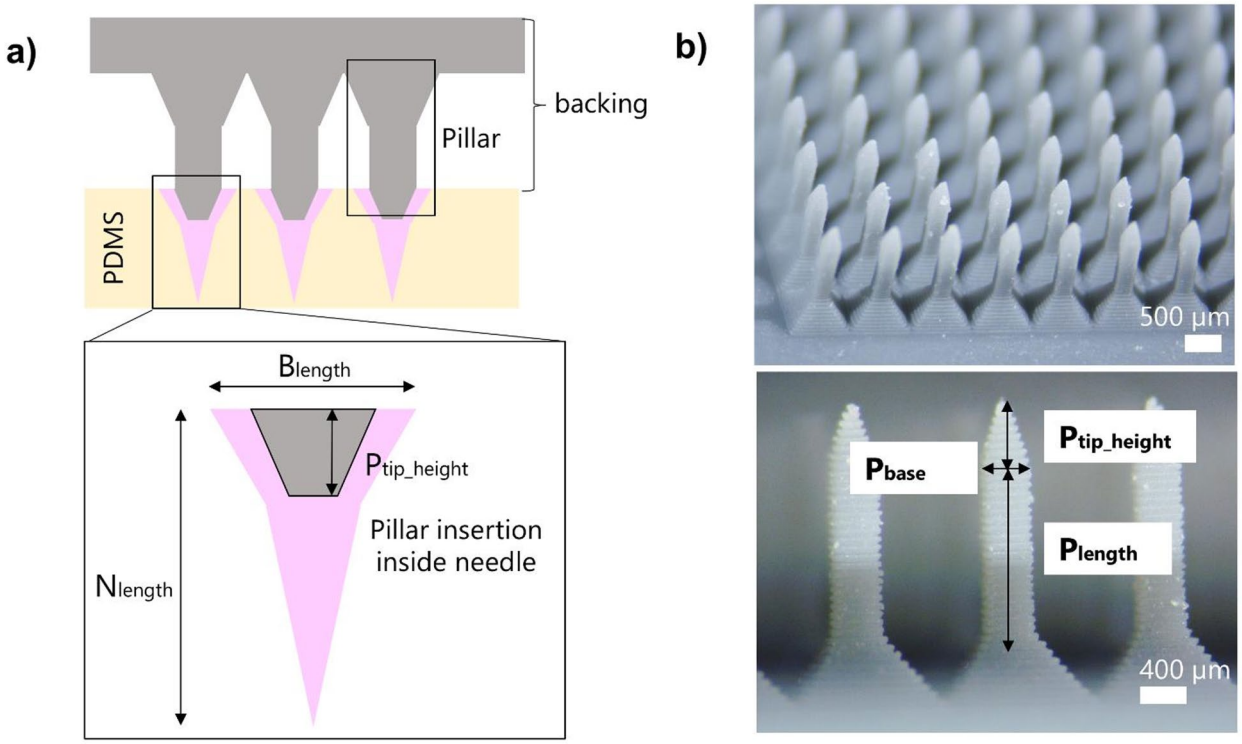

Fig. 3. Design and characteristic evaluation of backing. (**a**) Schematic design of the MAP and its 3D-printed backing layer. Cross-sectional schematics showing pillar position and microneedle tip-filling. (**b**) Optical microscopic images of the fabricated backing pillars.

Fabrication process of pillar guided MAP

A plasma-treated PDMS mold was filled with a 15% HA and r-DIs-S solution (1.0×10^8 PFU/mL), aligned with a prefabricated backing layer, and dried at 4 °C and 10% RH for 8 h. After complete drying, the backing layer was carefully removed from the PDMS mold (Fig. 4a). The fabricated MAP had a needle length (N_{length}) of 688 ± 25 μm and a base length (B_{length}) of 477 ± 31 μm ($n = 15$) (Fig. 4b). We confirmed that the tip parts were successfully attached to the pillars. However, we observed the formation of inter-needle bridging, which led to vaccine loss (Fig. 4c). This bridging formation resulted from solution dispensed onto the space between needle cavities. Future optimization of formulation viscosity, precise dispensing using a precision dispenser, and improved mold design may further minimize bridging formation.

We compared the drying kinetics of PG-MAP with those of conventional one-step molding methods using identical hyaluronic acid formulations (15% HA). The time required to reach 90% of total mass loss (t_{90}) was shorter for the pillar-guided (PG) method than the conventional one-step molding (OS) method under drying conditions (4 °C, ~10% RH). The PG method, which utilized 50 μL of vaccine solution per mold, achieved 90% mass loss (t_{90}) in 9 h, almost half faster than the 18.1 h required by the OS method using the 1 mL casting approach (Fig. 4d).

From the theoretical calculation method, the PG method delivered a tip-loading efficiency (TLE) of 16.5%, whereas the conventional OS method achieved only 2.0%. When expressed as a fold-change, the PG approach resulted in an 8.3-fold increase in TLE (Fig. 4e).

Our results demonstrated that shortening the drying time during MAP fabrication —achieved via the PG method—leads to improved preservation of viral titer, with a viability rate of 50.4%, compared to 40.4% for the conventional OS method (Fig. 4f). This enhanced stability can be attributed to the reduced exposure of the virus to prolonged osmotic pressure in the liquid phase, which minimizes viral degradation during fabrication[36]. The difference in viral titer between the two methods implied the critical importance of process optimization for vaccinia virus vaccine formulations. Thus, limiting the time, the virus remains in a liquid state by the pillar-guided method could preserve viral titer, which is essential for ensuring the feasibility in vaccine administration using MAPs. In addition, we acknowledge that the initially used 3D printed resin may not be optimal for biocompatibility. To address this, we will consider using a photopolymer resin specifically designed for biomedical applications, which is more suitable for skin contact.

Next, evaluation of mechanical strength demonstrated that all MAPs, regardless of HA concentration, exhibited failure forces sufficient for skin penetration (Fig. 4g, red dotted lines[37]. It is expected that this balance of high viral titer viability and mechanical performance highlights the promise of our pillar-guided fabrication approach for practical applications.

Release kinetics from the PG-MAP were evaluated using PBS(-) as the release medium, which was selected to mimic the physiological pH of interstitial fluids in transdermal application. The release profile of Rhodamine

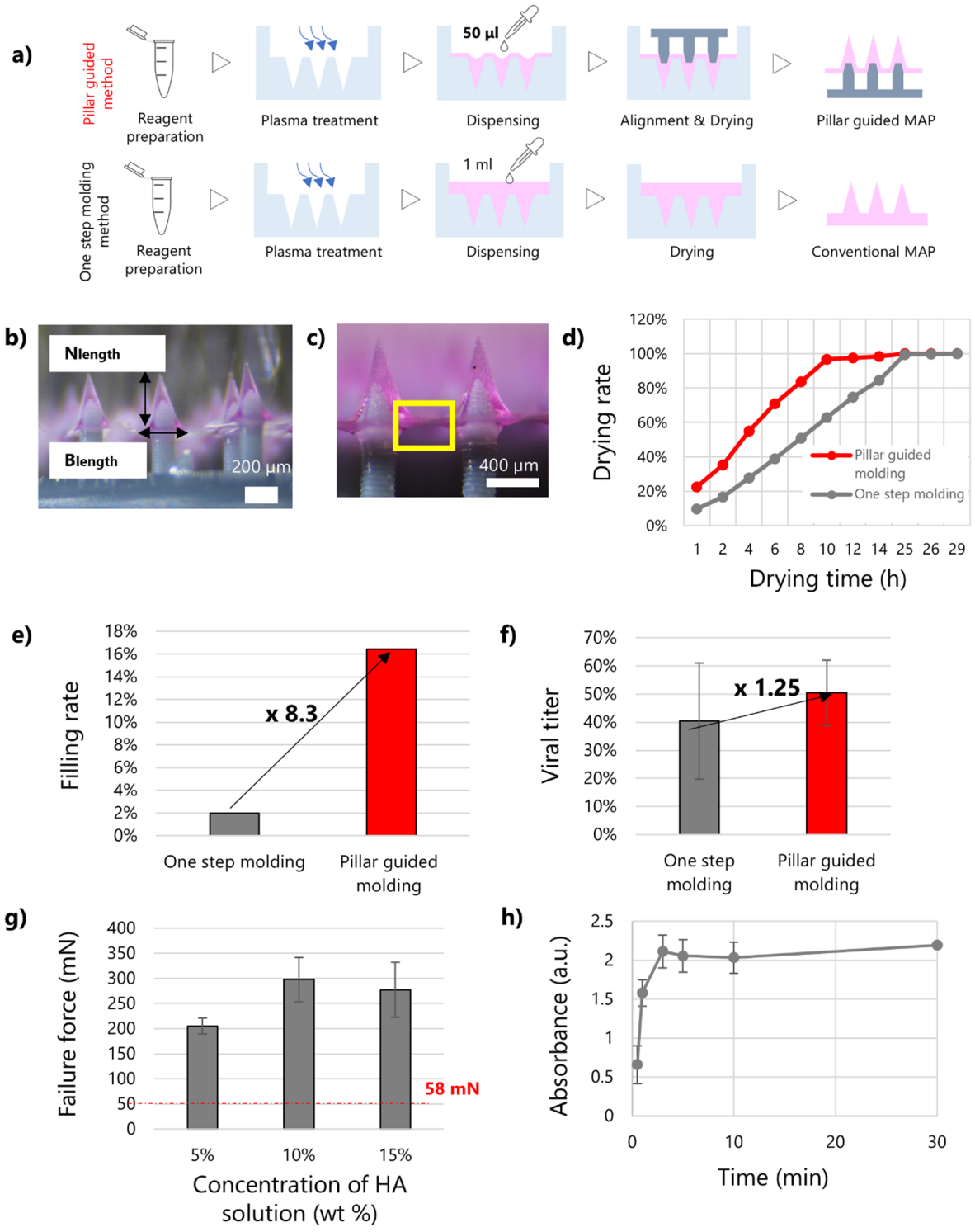

Fig. 4. Fabrication and characteristic evaluation of PG-MAP. (**a**) Schematic of PG-MAP mold and micro molding process. (**b**) Optical microscopic image of the fabricated PG MAP. (**c**) Optical microscopic image of PG-MAP showing needle alignment and formation of bridging. (**d**) Drying kinetics of pillar guided molding and conventional one-step molding. (**e**) Tip-loading efficiency (TLE) comparison between pillar guided molding and one-step molding. (**f**) Viral titer stability measured by plaque assay after fabrication, comparing the pillar-guided method (viability: 50.4%) with the conventional one-step molding method (viability: 40.4%), indicating enhanced preservation of viral titer with the PG approach ($n = 4$). (**g**) Axial force measurements confirming failure force of PG-MAP fabricated with hyaluronic acid (HA) at 5%, 10%, and 15% concentrations ($n = 5$), the red dotted lines, 58mN, indicate the threshold for skin puncture force[37] (**h**) Absorbance of Rhodamine B release from PG-MAP in PBS(-) solution at 37 °C, shown as function of time ($n = 4$).

B from the PG-MAP showed a burst release during the initial minutes of immersion. (Fig. 4h). This behavior indicates that the PG-MAP enables a rapid release of the payload, achieving the target delivery within several minutes after application. In the context of vaccinia virus vaccine administration, a rapid dissolving profile is considered advantageous, as it enhances user convenience and minimizes application time. Although in vivo insertion experiments in mice required approximately 5 min for complete dissolution of the patch, this minor deviation from measurements can be attributed to variations in skin hydration and interstitial fluid availability. Nevertheless, the reduced dissolution time observed in vitro suggests improved usability and emphasize the potential of PG-MAP for efficient and practical transdermal vaccine delivery.

In vivo immunogenicity and protection against SARS-CoV-2

To evaluate the immunogenicity of r-DIs-S loaded PG-MAP, BALB/c mice were immunized with two MAPs containing $9.4 \pm 1.8 \times 10^6$ PFU/patch (total dose per mouse: ~1.9×10^7 PFU), as confirmed by plaque assay, followed by a booster dose at week 4. Each MAP was applied to the dorsal skin for 5 min.

Vaccination protocol and dose delivery

The present study demonstrates the efficacy of r-DIs-S loaded PG-MAP vaccination in generating robust and durable immune responses in a murine model. By standardizing the vaccination procedure, including inoculation at identical dorsal sites, application of consistent pressure, and precise quantification of the delivered dose, we ensured a reliable assessment of immune responses with the PG-MAP. Vaccine efficacy was evaluated using BALB/c mice, which were intradermally immunized with r-DIs-S loaded PG-MAP or inoculated with PBS or DIs through skin scarification (Fig. 5a). Two separate vaccinations were administered four weeks apart, and a challenge was conducted at 16 weeks (Fig. 5b).

Puncture rates of 80% and 88% were calculated by counting needles remaining after puncture (Fig. 5c, Supplementary Information 2). We then evaluated the exact amount of viral titer loaded in the PG-MAP by plaque assay before vaccination. The PG-MAP was loaded with average values of $9.4 \pm 1.8 \times 10^6$ PFU/patch and $11.6 \pm 1.8 \times 10^6$ PFU/patch for the 1 st and 2nd vaccinations, respectively (Fig. 5d).

Following immunization, PG-MAP-vaccinated mice showed a stronger anti-DIs IgG response than those vaccinated using traditional scarification, with an average 1.2-fold increase in optical density observed over six weeks (Fig. 5e). Furthermore, PG-MAP vaccination uniquely induced spike protein–specific IgG (Fig. 5f), whereas no such antibodies were detected in mice inoculated by scarification or with PBS, underscoring the specific immunogenicity of PG-MAP vaccination.

Antibody responses against vaccinia and SARS-CoV-2 Spike

Dose-antibody analysis about the dose and related antibody indicated a correlation between the delivered r-DIs-S dose and antibody response. To quantify this relationship, we examined the extent to which a linear relationship could be confirmed using the correlation coefficient (R^2).

Dose–antibody correlation analysis revealed a strong positive relationship between the delivered r-DIs-S dose and early antibody titers at week 2. The correlation for total IgG ($R^2 \approx 0.83$; Fig. 5g) and spike-specific IgG was pronounced, indicating that higher antigen doses resulted in greater early stage immune activation. However, the r value declined (Fig. 5h) by weeks 4 and 6, suggesting the potential influence of booster effects and maturation of adaptive immune responses over time. Further studies are needed to clarify the contribution of maturation of adaptive immune responses, including antibody avidity maturation. These findings suggest that while early antibody production is closely tied to the administered dose, the immune system memory response and subsequent boosters play an increasingly dominant role as vaccination progresses. In summary, these results highlight the capacity of PG-MAP to deliver precise, and immunogenically effective r-DIs-S doses.

Protection against SARS-CoV-2 challenge

Next, we examined the protective efficacy of r-DIs-S loaded MAP against lethal challenge infection in BALB/c mice infected with the SARS-CoV B.1.351 variant (Fig. 6). The vaccinated mice were infected intranasally with the SARS-CoV-2 TY8-612 strain 10 weeks after the second vaccination. Both PBS- and DIs-inoculated mice rapidly lost weight after SARS-CoV-2 infection, and one DIs-inoculated mouse died on day 6 post-infection. By day 7 post-infection, three PBS- and three DIs-inoculated mice showed 30% or greater weight loss, accompanied by decreased activity. These mice were euthanized because they met the endpoint cutoff. In contrast, mice vaccinated with r-DIs-S loaded MAP recovered rapidly from weight loss following SARS-CoV-2 infection, and all PG-MAP-vaccinated mice survived and maintained their body weight throughout the study.

Lung viral titers, measured by plaque assay and RT-qPCR, were markedly reduced in the vaccinated group compared to the control group (Fig. 6c–d). On day 7 post-infection, the lung pathology of vaccinated mice was markedly ameliorated compared to that of control mice inoculated with PBS(-) or DIs. Histopathological analysis of lung sections revealed that PG-MAP-vaccinated mice exhibited preserved alveolar structures and minimal inflammation, whereas control mice showed widespread alveolar destruction and immune cell infiltration (Fig. 6e). These results suggest that vaccination with r-DIs-S MAP significantly reduced the pulmonary viral titer, thereby alleviating the severity of symptoms caused by infection with the SARS-CoV-2 TY8-612 strain.

Conclusion

In this study, we demonstrated the feasibility of administering recombinant vaccinia virus (r-DIs-S) vaccines using a pillar-guided microneedle array patch (PG-MAP). The pillar-guided fabrication method enabled the precise loading of viral solutions exclusively at the microneedle tips, resulting in a tip-loading efficiency of 16.5%, which represents an 8.3-fold increase compared to the conventional one-step molding method. After fabrication, a plaque assay confirmed that 50.4% of the initial viral titer was retained using the PG-MAP

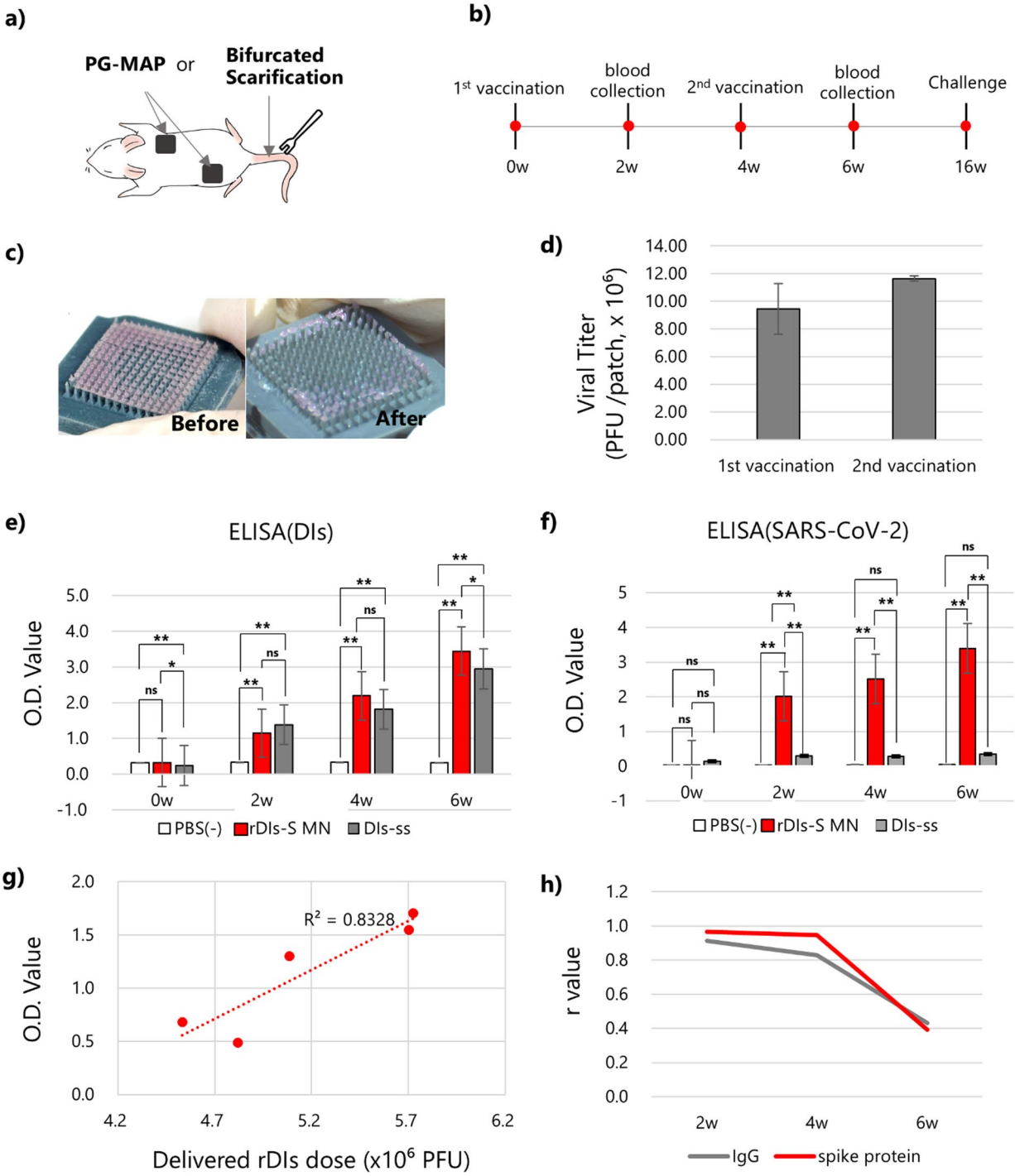

Fig. 5. In vivo delivery and immunogenicity of r-DIs-S loaded PG-MAPs. (**a**) Immunization protocol: comparison of intradermal r-DIs-S loaded PG-MAP application versus bifurcated needle scarification in BALB/c mice. (**b**) Schedule of vaccinations including blood collection, and viral challenge over a 16-week period. (**c**) Images of MAP before and after application to the mouse dorsal skin, demonstrating microneedle insertion. (**d**) Quantification of delivered r-DIs-S viral titer per patch, measured by plaque assay prior to each vaccination (mean ± SD, $n = 4$). (**e**) Time-course of anti-DIs IgG responses in mice measured by ELISA ($n = 5$). Mice vaccinated with r-DIs-S-loaded PG-MAPs developed significantly higher serum anti-vaccinia IgG titers than those receiving scarification with native DIs or PBS. P-values were calculated using one-way ANOVA ($^*p < 0.05$; $^{**}p < 0.01$; ns, not significant). (f) Time-course of r-DIs-S specific antibody responses in mice measured by ELISA ($n = 5$). Importantly, only the PG-MAP group elicited strong spike protein–specific IgG responses, indicating successful antigen expression from the r-DIs-S vector in vivo. P-values were calculated using one-way ANOVA ($^*p < 0.05$; $^{**}p < 0.01$; ns, not significant). (**g**) Correlation between delivered r-DIs-S dose with IgG response at week 2. (**h**) Temporal changes in the correlation coefficient (r) between the delivered dose and S protein–specific antibody responses across 6 weeks, reflecting the influence of immune memory and secondary responses following the booster.

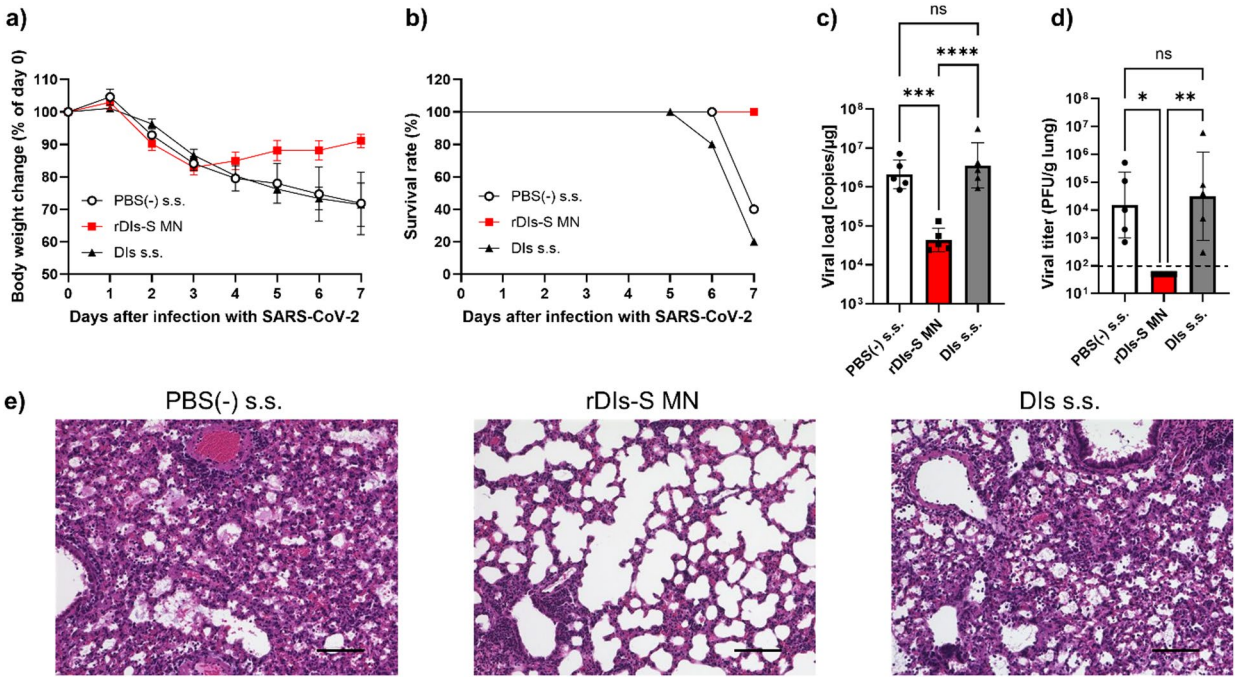

Fig. 6. Protective efficacy of r-DIs-S MAP against lethal infection with SARS-CoV-2 B. 1.351. (**a**) Temporal changes in the body weights of BALB/c mice with or without vaccination following infection with the SARS-CoV-2 TY8-612 strain. (**b**) Survival rate of BALB/c mice after SARS-CoV-2 infection. (**c**) Viral loads of left lung homogenates, determined via RT-qPCR for the SARS-CoV-2 N protein gene. P-values were calculated using one-way ANOVA, followed by Tukey's test (***$p < 0.001$; ****$p < 0.0001$; ns, not significant). (**d**) Infectious viral titers in left lung homogenates were measured by a plaque assay. The dashed line indicates the limit of detection (100 PFU/g lung). Viral titers below the LOD are represented as 50 PFU/g of lung tissue. P-values were calculated using one-way ANOVA, followed by Tukey's test (*$p < 0.05$; **$p < 0.01$; ns, not significant). (**e**) Representative sections (hematoxylin and eosin staining; section thickness: 4 μm) of the right upper lung lobes of SARS-CoV-2-infected BALB/c mice at 7 days post-infection (dpi). Scale bar: 100 μm.

method, compared to 40.4% using the conventional approach. This improvement was achieved by shortening the drying time to 9.7 h for the PG-MAP, compared to 18.1 h for the one-step method (both at 4 °C, 10% RH). Mechanical evaluations confirmed that the PG-MAPs possessed sufficient strength for intradermal application, with insertion rates ranging from 80% to 88% in the murine skin.

For immunogenicity studies, we used rDIs loaded PG-MAP with a viral titer of $9.4 \pm 1.8 \times 10^6$ PFU/patch for the first vaccination and $11.6 \pm 1.8 \times 10^6$ PFU/patch for the second vaccination. From this experiment, we demonstrated that r-DIs-S MAP vaccination induced robust anti-DIs IgG and SARS-CoV-2 spike-specific IgG responses. Mice immunized with r-DIs-S MAP showed a 1.2-fold higher anti-DIs IgG response than those immunized with the traditional scarification method over six weeks. Importantly, only the MAP-vaccinated group developed spike-specific antibodies, confirming in vivo expression of the SARS-CoV-2 antigen.

In a lethal SARS-CoV-2 challenge model, PG-MAP vaccinated mice exhibited 100% survival and complete protection, whereas all control animals succumbed to infection. These results quantitatively confirm that the PG- MAP platform enables precise, efficient, and immunogenically effective delivery of vaccinia virus vaccines with stable viral stability and reliable protective efficacy in vivo.

We expect that our developed PG-MAP system makes it a promising candidate for decentralized vaccination strategies, particularly under the limited cold-chain infrastructure and medical personnel. We believe that our technology may accelerate global immunization efforts against emerging infectious diseases.

Materials and methods

Preparation of vaccine solution

The recombinant vaccinia virus strain r-DIs-S, carrying the SARS-CoV-2 spike gene, was produced at the Tokyo Metropolitan Institute of Medical Science. (Tokyo, JAPAN). To prepare the vaccine solution, 30 wt% hyaluronic acid with a molecular weight of 14 kDa (Contipro a.s., Dolní Dobrouč, CZECH REPUBLIC) and 10% trehalose (T9531-10G, Sigma-Aldrich, St. Louis, USA) were added to a suspension of r-DIs-S virus (1.3×10^9 PFU/mL in DMEM (10569-010, Thermo Fisher Scientific, Waltham, US)), and the mixture was gently dissolved at 4 °C by pipetting.

To optimize the HA concentration, four formulations containing 5%, 10%, 15%, and 20% HA (w/v) were prepared. Trehalose was maintained at a constant concentration of 5% (w/v) across all formulations. HA powder was dissolved in Dulbecco's Modified Eagle Medium (DMEM) at 25 °C for 6 h, and the virus solution was added

to a final titer of 1×10^7 PFU/mL. Each 500 µL sample was transferred to sterile 1.5 mL microcentrifuge tubes and stored at 4 °C for 6 h. Viral titers were determined using a plaque assay.

To assess the effects of temperature on viral stability during MAP fabrication, 15% HA solutions containing r-DIs-S (initial titer: 1.0×10^5 PFU/mL) were prepared and stored at 4–25 °C for 6 h to simulate dispensing and drying conditions during MAP fabrication. After this incubation period, the samples were subjected to plaque assays.

Fabrication of PG-MAP

A 14 × 14 microneedle master mold was fabricated from tungsten carbide using electrical discharge machining (EDM). The mold geometry was confirmed by optical microscopy (VH-5500; Keyence, Osaka, JAPAN) and image analysis (Zeiss ZEN, Carl Zeiss AG, Oberkochen, GERMANY). A polydimethylsiloxane (PDMS) negative mold was cast from the master mold.

The MAP backing layer was designed using 3D CAD software (Fusion 360, version 2604.1.48, https://www.autodesk.com/products/fusion-360, Autodesk, Inc., San Francisco, USA) and fabricated using a stereolithography (SLA) 3D printer (Saturn 2, Elegoo, Shenzhen, CHINA) with a water-washable resin (8 K, Elegoo, Shenzhen, CHINA). After printing, the backings were rinsed in DI water and ethanol, UV-cured (Mercury Plus V2.0, Elegoo, Shenzhen, CHINA), and oven-dried at 40 °C for 1 h to remove residual photoinitiators. The dimensions were determined such that the top cover would fit inside the bottom mold, with the back-layer thickness of the MAPs ranging from 500 to 550 µm.

Next, a PDMS negative mold fabricated from the master mold was treated with air plasma (YHS-R, Sakigake, Tokyo, JAPAN) to enhance the adhesion between the viscous hyaluronic acid r-DIs-S solution and the PDMS mold surface. This plasma treatment was used to improve the wettability of the substrate with the vaccine solution. 50 µl of mixed formulation including 15 wt % HA and vaccinia virus (1.0×10^8 PFU mL^{-1}) solutions were then dispensed onto the plasma-treated PDMS mold. After aligning and positioning the prefabricated backing layer with an r-DIs-S solution-filled PDMS mold, the assembled patches were placed in a sealed container with a portable dehumidifier and dried in a refrigerator at 4 °C and 10% RH for 8 h to ensure complete microneedle drying. After complete drying, the backing layer was carefully removed from the PDMS mold.

All fabrication was performed in a biosafety cabinet (MHE-131AJ, Sanyo, Osaka, JAPAN) at 25 °C. MAPs were dried in a sealed container with a portable dehumidifier (MD-3, Toyo Living, Tokyo, JAPAN) at 4 °C for 8 h to ensure complete drying of the microneedles.

Drying kinetics: One-step vs. Pillar guided methods

To evaluate the drying kinetics, MAPs were fabricated using both conventional one-step molding and the pillar-guided method. A 15% HA solution was used. For one-step molding, 1.0 mL of solution was added to each PDMS mold, whereas for the pillar-guided method, only 50 µL was used. The mold–backing assemblies were weighed on an analytical balance (SECURA125-1SJP, Sartorius AG, Göttingen, GERMANY) to obtain the initial mass (m_0) at 1-h intervals. Drying time was defined as the duration required to achieve three consecutive weights varying by < 1 mg. The time to 90% mass loss (t_{90}) was estimated using linear interpolation (Supplementary Information 3). Samples ($n = 2$) were dried either in a refrigerated chamber at 4 °C (10% RH) or at room temperature (25 °C, 10% RH).

Theoretical Estimation of Tip-Loading efficiency (TLE)

Tip-loading efficiency (TLE) was calculated from the geometric parameters of the microneedle array, which means the calculations from the microneedle volume (V_{needle}) and total dispensed volume (V_{total}). The internal volume of a single microneedle (V_{needle}) was obtained from master mold parameters. V_{tips} is the total volume of 14 × 14 microneedle cavities, therefore

$$V_{tips} = 196 \times V_{needle}$$

TLE was then expressed as

$$TLE\ (t\%) = \frac{V_{tips}}{V_{total}} \times 100,$$

where V_{total} is the solution volume dispensed into the mold (1 mL for the one-step method and 50 µL for the pillar-guided method). This estimate assumes full cavity filling and no bridging.

Viral titer after MAP fabrication

To evaluate viral retention, the microneedles were fully dissolved in 1 mL of DMEM and incubated for 5 min at room temperature. The resulting solution was immediately used for plaque assays.

Mechanical strength testing

The mechanical failure forces of the microneedles were measured using a force gauge (MX2-500 N, Imada, Aichi, JAPAN). A compressive force was applied until individual needle failure was detected, ensuring penetration into the skin layer without breaking.

Kinetics release

PG-MAP were subjected to a release kinetics study. PG-MAP containing 1% (w/w) Rhodamine B were dissolved in 20 mL of PBS(-) pH 7.4 at 37 °C under stirring at 100 rpm to ensure uniform distribution and maintain

equilibrium conditions. At predetermined time points ranging from 0.5 to 30 min, 200 µL were collected for analysis. The concentration of the released Rhodamine B was measured by UV spectrophotometry (UV-2600, Shimadzu Corporation, Tokyo, Japan) within the 500–580 nm spectrum range. After each measurement, 200 µL of PBS(-) pH 7.4 solution was replaced within the sealed container to maintain a constant volume. Finally, the release profile was plotted with the y-axis representing the absorbance of rhodamine B as a function of time to visualize the dissolution behavior of the PG-MAP.

Plaque assay

Plaque assays for vaccine stability testing were performed as follows. Chicken embryonic cells (CRL-12203 UMNSAH/DF-1 cells, ATCC, Manassas, USA) were seeded in a 6-well plate at a density of 8×10^5 cells/well and incubated at 37 °C and 5% CO_2 in a humidified atmosphere for 24 h.

For each sample, the viral solution was serially diluted in a maintenance medium containing 2% fetal bovine serum (FBS) (A525671, Thermo Fisher Scientific, Waltham, US), and 100 µL of each viral solution was dispensed into the designated wells and incubated at 37 °C and 5% CO_2 in a humidified atmosphere for 1 h. Overlay medium (0.5%/MC/DMEM + GlutaMAX/5%FBS) was prepared from DMEM (10569-010, Thermo Fisher Scientific, Waltham, US) supplemented with Methylcellulose (22224-55, NACALAI TESQUE, Kyoko, JAPAN), 5% FBS (A525671, Thermo Fisher Scientific, Waltham, US), penicillin-streptomycin (PS) (15140-122, Thermo Fisher Scientific, Waltham, US), and HEPES(1 M) (15630-080, Thermo Fisher Scientific, Waltham, US) in distilled water). Overlay medium (2 mL/well) was added to each well of the titration plate and incubated at 37 °C in a 5% CO_2 incubator for 3 days.

The overlay medium was then carefully aspirated, and the cells in each well were gently washed with PBS. Cells were fixed by adding 2 mL of 10% neutral buffered formalin to each well and incubated in a biosafety cabinet for at least 1 h. Following fixation, formalin was carefully removed, and each well was washed twice with 1 mL of tap water. Subsequently, 2 mL of tap water was added to each well, the plate lids were opened, and the plates were exposed to UV light within a biosafety cabinet for 1 h to ensure viral inactivation. After UV treatment, crystal violet solution (2 mL) was added to each well and incubated at room temperature for 15 min. Virus dilution factors representing 5–100 plaques per well were identified, and the virus titer was calculated by counting the plaques.

Ethics statement

All animal experiments complied with the Science Council of JAPAN's and ARRIVE guidelines for the proper conduct of animal research. Protocols were approved by the Animal Care and Use Committee of the Tokyo Metropolitan Institute of Medical Science (Approval No. 24–071).

Animal vaccination

Negative BALB/c mice (8 weeks old; JAPAN SLC Inc.) were maintained under a 12-h light/dark cycle with ad libitum access to food and water. The mice were anesthetized with intraperitoneal ketamine/xylazine (150 µL) and shaved dorsally.

A pre-vaccination blood sample (50 µL) was collected from the retro-orbital venous plexus, and the baseline serum was separated and stored at −20 °C.

Fifteen mice were randomly assigned to three groups ($n = 5$ per group). In the first control group, mice received 5 µL of sterile phosphate-buffered saline (PBS) via skin-scarification. In the second group, two MAPs containing ($6.14–6.78 \times 10^6$ PFU) recombinant vaccinia virus DIs strains carrying the SARS-CoV-2 S gene (r-DIs-S) were applied to the shaved dorsal skin (one patch on the right upper quadrant and one on the left lower quadrant) for 5 min. In the third group, mice received 1×10^7 PFU of the DIs virus in 5 µL via skin scarification.

After PG-MAP application, the PG-MAP was carefully removed. The PG-MAP before and after insertion was observed under a microscope to count the number of microneedles retained in the patch versus those inserted into the skin. The puncture rate was calculated, and the delivered dose was estimated based on the initial number of microneedles and the virus titer. Viral titers in the dissolved microneedles (after patch retrieval) were evaluated using a plaque assay, as described previously. The second vaccination was administered at week 4 using the same procedure. Additional blood samples were collected from the submandibular vein at Weeks 0,2,4 and 6 for immunological analysis.

Evaluation of immunogenicity

To assess the immune induction after vaccination, we performed the following experiments.

Enzyme-linked immunosorbent assay (ELISA)

IgG responses against inactivated r-DIs and SARS-CoV-2 spike proteins were quantified using standard ELISA protocols. Plates were coated with NP40-inactivated DIs or recombinant S protein (Acro, SPN-C52H8), followed by blocking, incubation with diluted serum, secondary HRP-conjugated antibody, substrate development (OPD), and absorbance measurement at 492 nm. Details are as follows. DIs virus was grown in primary chicken fibroblasts and purified using OptiPrep™ (Iodixanol) density gradient medium and ultracentrifugation. Purified DIs were suspended in PBS and inactivated with 0.2% NP40. The inactivated DIs solution was coated onto 96-well round-bottom plates and incubated overnight at 4 °C. For IgG detection against the SARS-CoV-2 spike protein, 96-well plates were coated by incubating them overnight at 4 °C with 1 µg/mL of recombinant C-terminus His-tagged spike protein of the early pandemic strain of SARS-CoV-2 (Acro, #SPN-C52H8) dissolved in 50 mM carbonate buffer (pH 9.6). The plates were blocked with 1% BSA in PBS(-), containing 0.5% Tween20 and 2.5 mM ethylene diaminetetra-acetic acid, followed by incubation with a 100- or 1000-fold dilution of sera collected from vaccinated mice. After extensive washing, the plates were incubated with horseradish peroxidase-

conjugated goat anti-mouse IgG polyclonal antibody (62–6520, Thermo Fisher Scientific, Waltham, MA, US). Next, 100 µL of a mixture of o-phenylenediamine dihydrochloride and hydrogen peroxide (H_2O_2) in citrate–phosphate buffer was added to each well. The reactions were quenched by adding 1 M sulfuric acid, and the absorbance was measured at 492 nm wavelength.

In vitro neutralization assay for vaccinia virus

To assess neutralizing antibody activity, mouse sera were heat-inactivated at 56 °C for 30 min. Serial dilutions of heat-inactivated sera were mixed with equal volumes of 3000 PFU/mL DIs and incubated at 37 °C overnight. DF-1 cells were then infected with 30 µL of the virus/serum mixture in 24-well plates. At 96 h after infection, the neutralization titer was expressed as the reciprocal of the maximum dilution of serum at which the plaque numbers were reduced by 50% compared to those in wells infected with the virus alone (without serum).

Challenge experiment with SARS-CoV-2

Ten weeks after the 2nd vaccination, the mice were inoculated intranasally with the SARS-CoV-2 TY8-612 strain (GISAID ID: EPI_ISL_1123289), lineage B. 1. 351, provided by Dr. Masayuki Saijo, Mutsuyo Takayama-Ito, and Masaaki Satoh (Department of Virology 1, National Institute of Infectious Diseases)[38]. Each mouse received 1×10^5 PFU in a 50 µL volume. Body weight was monitored daily, and mice that lost more than 30% of their initial body weight were humanely euthanized and recorded as deceased.

The animal was euthanized by cervical dislocation immediately after blood collection via cardiac puncture under isoflurane anesthesia. Subsequently, the lungs were harvested via thoracotomy. The collected blood was centrifuged (15,000 rpm, 5 min, RT), and the serum was recovered. Both the serum and lungs were stored at − 80 °C until use.

Determination of infectious SARS-CoV-2 titer

Infectious SARS-CoV-2 titers (viral loads) were determined using a standard plaque assay. Briefly, the left lung lobes were harvested, homogenized, and centrifuged. The supernatants were stored at − 80 °C. Infectious titers were determined by plaque assay on Vero E6/TMPRSS2 cells using 0.6% agarose overlays and crystal violet staining. The details are as follows. The left lung lobe from each necropsied mouse was weighed and homogenized in nine volumes of Hanks-balanced saline solution (Thermo Fisher Scientific, Waltham, MA, USA) using a Multi-Beads Shocker (YASUI KIKAI, Osaka, JAPAN). Homogenates were centrifuged at 3000 × g for 10 min at 4 °C. The supernatant was collected and stored at − 80 °C until further use. For the plaque assay, serial tenfold dilutions of the supernatant (100 µL per well) were inoculated onto confluent monolayers of Vero E6/TMPRSS2 cells in a 6-well plate and incubated at 37 °C for 1 h. Unbound viruses were removed by washing the cells with DMEM. The cells were then overlaid with DMEM containing 10% FBS and 0.6% agarose (Sigma-Aldrich, St. Louis, MO, USA). After 72 h of incubation at 37 °C, the cells were fixed in 10% neutral buffered formalin and stained with 1% crystal violet. The titer of SARS-CoV-2 was defined as plaque-forming units per gram of lung tissue (PFU/g lung), with a detection limit of 100 PFU/g lung.

SARS-CoV-2 RNA quantification

Total RNA was extracted from 70 µL of the supernatant from lung homogenates prepared for the Plaque Assay (see plaque assay) using RNeasy Mini kits (Qiagen, Hilden, GERMANY) according to the manufacturer's instructions. RT-qPCR targeting the SARS-CoV-2 N gene was performed using a CDC primer/probe set (N2-F, N2-R, and N2-P). Fifty nanograms of total RNA was used to quantify the SARS-CoV-2 N protein gene[39]. The primers and probe used were as follows: forward primer 5'- TTACAAACATTGGCCGCAAA-3' (2019-SARS-CoV-2_N2-F), reverse primer 5'- GCGCGACATTCCGAAGAA-3' (2019-SARS-CoV-2_N2-R), and probe 5'-FAM- ACAATTTGCCCCCAGCGCTTCAG-BHQ1-3' (2019-SARS-CoV-2_N2-P). Viral RNA quantification was performed using a 1-step reverse transcription-quantitative polymerase chain reaction (RT-qPCR), as previously described[38]. Viral loads were calculated as Log_{10} copies per microgram of total RNA.

Lung histopathology

The upper lobe of the right lung from each necropsied mouse was fixed in 10% neutral buffered formalin, embedded in paraffin, sectioned to a thickness of 4 µm, stained with hematoxylin and eosin (H&E), and subjected to routine histological examination. Images of H&E-stained sections were obtained using an all-in-one fluorescence microscope (BZ-X710, KEYENCE, Osaka, JAPAN) equipped with a Plan Apo 20x Lambda objective (NA0.75, Nikon, Tokyo, JAPAN).

Statistical analysis

Data plotted on a linear scale are expressed as the mean ± standard deviation (SD), while those plotted on a logarithmic scale are expressed as the geometric mean ± geometric SD. Inferential statistical analyses were performed using one-way ANOVA, followed by Tukey's test, as appropriate. Statistical significance was set at $p < 0.05$. All analyses were conducted using the Prism software package (version 10.4.2, https://www.graphpad.com, GraphPad Software, Inc., Boston, USA).

Data availability

The data that support the findings of this study are available from the corresponding author upon reasonable request.

Received: 1 July 2025; Accepted: 14 November 2025

Published online: 29 December 2025

References

1. Jackson, L. A. et al. An mRNA vaccine against SARS-CoV-2 — preliminary report. *N. Engl. J. Med.* **383**, 20 (2020).
2. Folegatti, P. M. et al. Safety and immunogenicity of the ChAdOx1 SARS-CoV-2-19 vaccine against SARS-CoV-2: a preliminary report of a phase 1/2, single-blind, randomised controlled trial. *Lancet* **396**, 10249 (2020).
3. Jara, A. et al. Effectiveness of an inactivated SARS-CoV-2 vaccine in Chile. *N. Engl. J. Med.* **385**, 10 (2021).
4. Ishigaki, H. et al. An attenuated vaccinia vaccine encoding the severe acute respiratory syndrome coronavirus-2 spike protein elicits broad and durable immune responses, and protects cynomolgus macaques and human angiotensin-converting enzyme 2 transgenic mice from severe acute respiratory syndrome coronavirus-2 and its variants. *Frontiers Microbiology* **13**, 967019, pp1-18 (2022).
5. Altenburg, A. F. et al. Modified vaccinia virus Ankara (MVA) as production platform for vaccines against influenza and other viral respiratory diseases. *Viruses* **6**, 273–295 (2014).
6. Tagaya, I. et al. A new mutant of dermovaccinia virus. *Nature* **192**, 381 (1961).
7. Ishii, K. & Moss, B. Mapping interaction sites of the A20R protein component of the vaccinia virus DNA replication complex. *Virology* **303**, 319–329 (2002).
8. Kitabatake, M. et al. SARS-CoV Spike protein-expressing Recombinant vaccinia virus efficiently induces neutralizing antibodies in rabbits pre-immunized with vaccinia virus. *Vaccine* **25**, 703–711 (2006).
9. Flynn, P. M. et al. Influence of needle gauge in Mantoux skin testing. *Chest* **106**, 1463–1466 (1994).
10. Hawkridge, A. et al. Efficacy of percutaneous versus intradermal BCG in the prevention of tuberculosis in South African infants: randomised trial. *BMJ* 337, a (2008). (2052).
11. Kim, Y. C. et al. Delivery systems for intradermal vaccination. In *Current Topics in Microbiology and Immunology* 77–112 (Springer, 2011).
12. Hegde, N. R., Kaveri, S. V. & Bayry, J. Recent advances in the administration of vaccines for infectious diseases: microneedles as painless delivery devices for mass vaccination. *Drug Discovery Today*. **16**, 1041–1049 (2011).
13. Mistilis, M. J. et al. Long-term stability of influenza vaccine in a dissolving microneedle patch. *Drug Delivery Translational Res.* **7**, 195–205 (2017).
14. Mistilis, M., Bommarius, A. S. & Prausnitz, M. R. Development of a thermostable microneedle patch for influenza vaccination. *J. Pharm. Sci.* **104**, 740–749 (2014).
15. Zhu, Z. et al. Transcutaneous immunization via rapidly dissolvable microneedles protects against hand-foot-and-mouth disease caused by enterovirus 71. *Journal Controlled Release* **243**, 291-302 (2016).
16. Ita, K. Transdermal delivery of drugs with microneedles: strategies and outcomes. *Journal Drug Delivery Sci. Technology* **29**, 16-23 (2015).
17. Matsuo, K. et al. Frontiers of transcutaneous vaccination systems: novel technologies and devices for vaccine delivery. *Vaccine* **31**, 2546–2554 (2013).
18. Larrañeta, E. et al. Microneedles: a new frontier in nanomedicine delivery. *Pharm. Res.* **33**, 1055–1073 (2016).
19. Tuan-Mahmood, T. M. et al. Microneedles for intradermal and transdermal drug delivery. *Eur. J. Pharm. Sci.* **50**, 623–637 (2013).
20. Larrañeta, E. et al. Microneedle arrays as transdermal and intradermal drug delivery systems: materials science, manufacture and commercial development. *Mater. Sci. Engineering: R: Rep.* **104**, 1–32 (2016).
21. Van der Maaden, K. et al. Microneedle-based drug and vaccine delivery via nanoporous microneedle arrays. *Drug Delivery Translational Res.* **5**, 285–296 (2015).
22. Sullivan, S. P. et al. Dissolving polymer microneedle patches for influenza vaccination. *Nat. Med.* **16**, 915–920 (2010).
23. Rodgers, A. M., Cordeiro, A. S. & Donnelly, R. F. Technology update: dissolvable microneedle patches for vaccine delivery. *Med. Devices (Auckland NZ)*. **12**, 351–358 (2019).
24. Chen, J. et al. Fabrication of tip-dissolving microneedles for transdermal drug delivery of meloxicam. *AAPS PharmSciTech*. **19**, 1023–1031 (2017).
25. Lee, I. C. et al. Fabrication of two-layer dissolving Polyvinylpyrrolidone microneedles with different molecular weights for in vivo insulin transdermal delivery. *RSC Adv.* **7**, 47020–47027 (2017).
26. Li, S., Xia, D. & Prausnitz, M. R. Efficient drug delivery into skin using a biphasic dissolvable microneedle patch with water-insoluble backing. *Adv. Funct. Mater.* **31**, 2103359 (2021).
27. Wang, Q. L. et al. Microneedles with controlled bubble sizes and drug distributions for efficient transdermal drug delivery. *Sci. Rep.* **6**, 38755 (2016).
28. Chu, L. Y. & Prausnitz, M. R. Separable arrowhead microneedles. *J. Controlled Release*. **149**, 242–249 (2011).
29. Shchelkunov, S. N. et al. Effect of the route of administration of the vaccinia virus strain LIVP to mice on its virulence and immunogenicity. *Viruses* **12**, 80795 (2020).
30. WHO. Summary report on first, second and third generation smallpox vaccines. *Medicine, Corpus ID 41122351, 1-33* (2013).
31. Frey, S. E. et al. Clinical responses to undiluted and diluted smallpox vaccine. *N. Engl. J. Med.* **356**, 1275–1284 (2002).
32. Frey, S. E. et al. Comparison of lyophilized versus liquid modified vaccinia Ankara (MVA) formulations and subcutaneous versus intradermal routes of administration in healthy vaccinia-naïve subjects. *Vaccine* **33**, 5225 (2015).
33. Frey, S. E. & Goll, J. Erythema and induration after Mpox(JYNNEOS) vaccination revisited. *N. Engl. J. Med.* **388**, 1432 (2023).
34. Bonfante, G. et al. Comparison of polymers to enhance mechanical properties of microneedles for bio-medical applications. *Micro Nano Syst. Lett.* **8** (8), 1 (2020).
35. Yim, S. G. et al. Low-temperature multiple micro-dispensing on microneedles for accurate transcutaneous smallpox vaccination. *Vaccine* **10**, 40561 (2022).
36. Coleman, H. et al. Effect of mechanical stresses on viral capsid disruption during droplet formation and drying. *Colloids Surf., B.* **233**, 113661 (2023).
37. Park, J. H. Biodegradable polymer microneedles: fabrication, mechanics and transdermal drug delivery. *J. Controlled Release*. **104**, 51–66 (2005).
38. Yasui, F. et al. Infection with the SARS-CoV-2 B.1.351 variant is lethal in aged BALB/c mice. *Sci. Rep.* **12**, 8104 (2022).
39. Lu, X. et al. US CDC real-time reverse transcription PCR panel for detection of severe acute respiratory syndrome coronavirus 2. *Emerg. Infect. Dis.* **26**, 1643–1645 (2020).

Author contributions

K.S., J.P., M.K., B.K. conceived the presented idea and concept of this study. K.S., J.P., H.A., F.Y., M.K., B.K. designed and carried out experiments and evaluations. K.S., J.P., H.A., F.Y., M.K., B.K. analyzed and discussed collected data. K.S., J.P. wrote the initial draft. K.S., J.P., H.A., F.Y., M.K., B.K. reviewed and revised the manuscript. B.K. supervised the project. All authors reviewed the results and approved the final manuscript.

Funding
This research was partially supported by AMED under Grant Number JP223fa627001 (UTOPIA Young Researcher Development Program), and partially by JST SPRING, Grant Number JPMJSP2108.

Declarations

Competing interests
The authors declare no competing interests.

Additional information
Supplementary Information The online version contains supplementary material available at https://doi.org/10.1038/s41598-025-29183-z.

Correspondence and requests for materials should be addressed to B.K.

Reprints and permissions information is available at www.nature.com/reprints.

Publisher's note Springer Nature remains neutral with regard to jurisdictional claims in published maps and institutional affiliations.